Contrib Mineral Petrol (2007) 154:135–151
DOI 10.1007/s00410-007-0183-y

ORIGINAL PAPER

Depleted and enriched mantle processes under the Rio Grande rift: spinel peridotite xenoliths

Y. Kil · R. F. Wendlandt

Received: 31 May 2006 / Accepted: 25 January 2007 / Published online: 17 February 2007

Abstract Upper mantle xenoliths from the southern Rio Grande rift axis (Potrillo and Elephant Butte) and flank (Adam's Diggings) have been investigated to determine chemical depletion and enrichment processes. The variation of modal, whole rock, and mineral compositions reflect melt extraction. Fractional melting is the likely process. Fractional melting calculations show that most spinel peridotites from rift axis locations have undergone <5% melting versus 7–14% melting for xenoliths from the rift shoulder, although the total range of fractional melting overlaps at all three locations. In the rift axis, deformed (equigranular and porphyroclastic texture) spinel peridotites are generally characterized by significantly less fractional melting (2–5%) than undeformed (protogranular) xenoliths (up to 16%). This difference may reflect undeformed xenoliths being derived from greater depths and higher temperatures than deformed rocks. Spinel peridotites from the axis and shoulder of the Rio Grande rift have undergone mantle metasomatism subsequent to melt extraction. Under the rift shoulder spinel peridotites have undergone both cryptic and patent (modal) metasomatism, possibly during separate events, whereas the upper mantle under the rift axis has undergone only cryptic metasomatism by alkali basaltic magma.

Introduction

Investigations of the deep-seated xenoliths of ultramafic rock in alkaline basalts, kimberlites, and the lamprophyre clan, have been important for understanding the physical state, chemical composition, and mineralogy of the upper mantle since isotopic and microanalytic instrumentation became widely available in the 1970s (Brown and Mussett 1981; Maaløe and Aoki 1977). Even though volcanic materials associated with continental rifting provide a window into the physical-chemical state of the mantle (e.g., Wendlandt et al. 1995), xenoliths in rift zones, compared with other tectonic zones, have not been systematically studied to understand upper mantle composition and properties or mantle processes related to plate movements (Bonatti et al. 1986; Nixon 1987; Witt-Eickschen and Seck 1987; Gamble et al. 1988; Zipfel and Wörner 1992).

Xenolith occurrences in the Rio Grande rift that were included in this study are Potrillo and Elephant Butte, located within the rift axis, and Adam's Diggings, located 100 km west of the rift axis (Fig. 1). Xenolith-bearing alkaline basaltic lavas were emplaced near Adam's Diggings, western New Mexico, on the western margin of the Rio Grande rift between about 13 and 6 Ma (Baldridge et al. 1991). Xenoliths from Elephant Butte, located within the rift axis, occur in basanitic and alkali basaltic lavas comprising an

---

Communicated by T.L. Groove.

Y. Kil (✉) · R. F. Wendlandt
Department of Geology and Geological Engineering,
Colorado School of Mines, Golden, CO 80401, USA
e-mail: basaltkil@yahoo.com

R. F. Wendlandt
e-mail: rwendlan@mines.edu

Y. Kil
New Ventures, Korea National Oil Corporation,
1588-14 Gwanyang-dong, Dongan-gu, Anyang,
Gyeonggi-do 431-711, South Korea

Fig. 1 The xenolith study areas in relation to the Rio Grande rift. *Stars* indicate sampling sites. After Baldridge et al. (1984)

extensive Quaternary volcanic field dated younger than 5 Ma (Warren 1978; Warren et al. 1979; Bachman and Mehnert 1978). Xenoliths were collected from three sampling sites, the Walnut Canyon, Black Mesa, and Red Cliff flows. The Potrillo Volcanic Field is a large occurrence of basanitic and alkali basaltic lavas and cinder cones that lies within the axis of the Rio Grande rift in southernmost New Mexico. Kilbourne Hole, Hunts Hole, and Potrillo Maar are volcanic maars within the Potrillo Volcanic Field. Kilbourne Hole, the location of xenoliths for this study, contains a larger variety of crustal and mantle xenoliths [associated with basanitic lavas dated at 80(±10) ka] than the other maars (Bussod and Williams 1991).

In a previous study, Kil and Wendlandt (2004) investigated spinel peridotite xenoliths from these three occurrences to determine pre-eruptive pressure and temperature conditions, xenolith textural attributes and extraction depths, and thermal history of the upper mantle. They documented a sequence of three different texture types, from protogranular through porphyroclastic to equigranular, with decreasing depth of origin and increasing shear deformation: Protogranular, porphyroclastic, and equigranular textured spinel peridotites originate at depths greater than 48, 48–42, and 42–26 km, respectively, at Potrillo, from greater than 38, 38–36, and 36–29 km, respectively, at Elephant Butte, and porphyroclastic texture spinel peridotites from Adam's Diggings originate at depths between 39–60 km. Based on xenolith textures and extraction depths, Kil and Wendlandt (2004) inferred the lithosphere-asthenosphere boundaries to be 48, 38, and ~60 km for Potrillo, Elephant Butte, and Adam's Diggings, respectively. Given this framework for the physical state of the mantle under the southern Rio Grande rift, the current investigation involves studies of xenoliths from these three locations to understand the chemical evolution of the mantle underlying the Rio Grande rift.

Analytical method

Glass beads were prepared from whole-rock powders for analysis using laser ablation-inductively coupled plasma mass spectrometry (LA-ICPMS) and EPMA (Nicholls 1974; Fedorowich et al. 1993; Stix et al. 1995). To avoid contamination, at least 0.5 cm of the outer xenolith surface that may have contained host basalt or weathering products was rejected. The remaining material was crushed in a steel mortar and a split was ground in an agate mill for whole-rock analyses. Glass beads were prepared using the following procedure: (1) 0.5 g of sample and 1.0 g of flux, consisting of 6.0 parts $Li_2B_4O_7$, 0.7 parts Li_2CO_3, and 3.3 parts $LiOH{\cdot}5H_2O$, were weighed into disposable 10 ml polycarbonate titration cups. (2) Powers were mixed and transferred to graphite crucibles. (3) The graphite crucibles were placed in a high temperature furnace and the temperature was slowly increased to avoid rapid decarbonation and dehydration of Li_2CO_3 and $LiOH{\cdot}5H_2O$. (4) Graphite crucibles were maintained at 1,120°C for 1 h with gentle slurrying every 10 min to hasten the melting and homogenize the melt composition. (5) Graphite crucibles were subsequently removed and allowed to cool rapidly to room temperature. Line scans of glass beads for selected elements using EPMA and LA-ICPMS documented homogeneous compositions.

Major, minor, and trace element concentrations in the glass beads were subsequently obtained using EPMA and LA-ICPMS. A CAMECA MBX microprobe at Colorado School of Mines was used to determine major element and selected minor element whole rock and mineral compositions. Glass bead whole-rock compositions were analyzed with 15 kV acceleration voltage, 15 nA beam current, and 50 μm beam size. Cr, Mn, Ni glass and basalt glass standards were used to minimize matrix effects. Count times were 20–40 s for major elements and 40–100 s for minor elements. All glass beads were analyzed in triplicate and the average taken. The concentrations of reported major element oxides are 1–3% relative uncertainty (two sigma). Two samples, spinel lherzolite (89EB19) and host rock (KB168), were analyzed by XRF at New Mexico Institute of Mining and Technology in Socorro, New Mexico, for normalization of EPMA whole-rock analyses. All elements analyzed by both methods are well matched (Kil 2002).

Mineral compositions were analyzed with the same EPMA and analytical conditions except for a 2–3 μm beam diameter. Olivine, orthopyroxene, and clinopyroxene grains were handpicked and analyzed separately, and small size spinel and phlogopite grains were analyzed in the thin section. Details of mineral analytical methods and results of mineral analyses are presented in Kil and Wendlandt (2004).

The LA-ICPMS at the United States Geological Survey (USGS) in Lakewood, Colorado, was used to determine trace element whole-rock and clinopyroxene compositions. Clinopyroxene grains were handpicked and analyzed separately. The LA-ICPMS is equipped with a Nd:YAG laser (266 nm UV laser; CETAC LSX-200) and Perkin-Elmer ELAN 6000 ICPMS (Lichte 1995; Ridley and Lichte 1998). The Nd:YAG laser was operated at 20 Hz and 50 μm spot size. All samples were analyzed in triplicate and the average taken. The USGS GSE standard was used for standardization. Clinopyroxene and whole-rock analyses were normalized to calcium contents, determined by EPMA. The concentrations of trace elements (above the 1 ppm) and rare earth elements (above the 0.1 ppm) are 1–4 and 2–20% relative uncertainty (2 sigma), respectively.

Petrography

Modal compositions of xenoliths were determined by point counting, using a variable grid spacing chosen to minimize counting errors (Solomon 1963). Investigated samples from all locations are spinel lherzolite and spinel harzburgite and texturally classified as protogranular, porphyroclastic, and equigranular based on the percentage of neoblasts and grain size (Kil and Wendlandt 2004): Protogranular rocks are coarse grained (grain size greater than 1 mm); porphyroclastic rocks contain over 50% small polygonal neoblasts (0.1–0.4 mm) amid larger porphyroclasts; and equigranular rocks are completely recrystallized and fine grained (grain size less than 1 mm). Textures ranging from protogranular through porphyroclastic to equigranular with kink banding of olivine, triple junctions with angular grain boundaries, and neoblastic olivine and orthopyroxene, indicate a dynamic evolution of mantle under the Rio Grande rift involving lithosphere attenuation and asthenosphere upwelling.

Only porphyroclastic spinel peridotites that have undergone an intermediate amount of deformation occur at the Adam's Diggings site on the rift shoulder. Phlogopite is present in the spinel harzburgites at this location and interpreted as having grown prior to deformation based on the presence of undulatory extinction and kink banding in the grains. The development of pyroxene exsolution lamellae prior to xenolith ascent to the surface indicates that the mantle experienced a cooling event (Kil and Wendlandt 2004). The sharp boundaries of olivine xenocrysts in the host basalt and between xenoliths and host basalt imply that xenoliths ascended rapidly from mantle to surface.

Representatives of all three texture types are found in spinel peridotites from the rift axis locations (Elephant Butte and Potrillo). Geothermobarometry results in Kil and Wendlandt (2004) and a website (http://www.my.netian.com/~ywkil) indicate that equigranular xenoliths from the rift axis (Elephant Butte and Potrillo) have undergone extreme deformation at relatively low temperatures and shallow depths, whereas protogranular xenoliths from the rift axis have undergone only slight deformation at relatively high temperatures and greater depths. Intermediate deformed porphyroclastic xenoliths from the rift axis originate at intermediate temperatures and depths. These three textural types are believed to be produced by extension and asthenospheric mantle upwelling along the rift axis as proposed by Baldridge et al. (1995). There are no hydrous minerals occurring in xenoliths from the rift axis sites. Pyroxene exsolution lamellae, observed in both undeformed (protogranular texture) and deformed (porphyroclastic texture) xenoliths at the Elephant Butte and Potrillo localities, document that rift axis xenoliths also underwent a cooling event prior to ascent to the surface (Kil and Wendlandt 2004). Rapid xenolith ascent rates are inferred from the absence of textural evidence of xenolith-magma interactions and diffusion modeling of Ca composition gradients at rims of olivine grains that suggests short duration heating events associated with xenolith transport (Kil and Wendlandt 2004).

Geochemistry

Whole-rock geochemistry

Representative whole-rock analyses of xenoliths are given in Table 1. Xenoliths from Adam's Diggings, Elephant Butte, and Potrillo are characterized by extensive variation in MgO from 38 to 45, 39 to 44, and 37 to 45 wt%, respectively (Fig. 2). SiO_2 and FeO (total) contents decrease slightly with increasing MgO content, but there is scatter to these trends. CaO, Al_2O_3, and TiO_2 contents also decrease with increasing MgO as would be expected for removal of a basaltic component (Frey and Green 1974, Griffin et al. 1998). The scatter of low Na_2O and K_2O contents may be explained by analytical uncertainty, migration of volatile elements caused by the EPMA electron beam, volatilization from the graphite crucible during prep-

Table 1 Major element analyses (wt%) of representative Rio Grande rift xenoliths and xenolith host rocks

Sample rock name location texture	ADTM1-1 Sp-Lh AD PO	ADTM6 Sp-Lh AD PO	ADTM7 Sp-Ha AD PO	ADTM18 Sp-Ha AD PO	ADTM27 Sp-Lh AD PO	ADTM34 Sp-Ha AD PO	EBBB2 Sp-Ha EB PR	EB4-1 Sp-Lh EB PR	89EB19 Sp-Lh EB PO	EBBM1-2 Sp-Lh EB PO
SiO_2	45.52	45.38	47.13	44.62	45.37	44.78	44.23	43.01	44.74	44.33
TiO_2	0.06	0.07	0.07	0.14	0.20	0.02	0.01	0.03	0.08	0.01
Al_2O_3	3.15	3.38	2.74	1.44	2.87	2.05	1.74	2.94	2.97	3.66
FeO	8.36	8.51	7.25	7.28	8.49	8.14	8.60	10.76	8.34	8.13
MnO	0.13	0.25	0.18	0.14	0.16	0.11	0.11	0.02	0.13	0.12
MgO	40.52	39.72	38.14	44.96	39.87	42.97	44.13	42.05	41.32	41.14
CaO	2.11	2.76	3.35	1.09	2.70	1.98	1.27	3.35	2.41	2.37
Na_2O	0.28	0.21	0.54	0.28	0.52	0.20	0.37	0.47	0.22	0.33
K_2O	0.06	0.01	0.04	0.04	0.09	0.05	0.04	0.03	0.03	0.03
P_2O_5	0.04	0.06	0.04	0.05	0.06	0.05	0.03	0.03	0.06	0.06
Total	100.24	100.35	99.48	100.05	100.31	100.36	100.53	102.69	100.30	100.17
Mg#	0.90	0.89	0.90	0.92	0.89	0.90	0.90	0.87	0.90	0.90

Sample rock name location texture	EBBM1-16 Sp-Lh EB PO	EBBM2-1 Sp-Lh EB PO	EBBB1 Sp-Lh EB PO	EBBB4 Sp-Lh EB PO	89EB23 Sp-Lh EB EQ	EBBB5 Sp-Ha EB EQ	EBW-2 Sp-Ha EB EQ	KB10 Sp-Lh PT PR	KB12 Sp-Lh PT PR	KB16 Sp-Lh PT PR
SiO_2	44.57	45.39	44.85	45.03	44.24	44.57	45.71	44.46	44.50	44.34
TiO_2	0.10	0.12	0.08	0.09	0.07	0.02	0.17	0.17	0.04	0.09
Al_2O_3	3.72	4.46	3.91	3.92	3.16	2.87	6.22	4.77	1.49	2.68
FeO	8.38	8.47	7.41	8.67	8.95	7.65	9.82	8.65	8.16	7.82
MnO	0.17	0.17	0.06	0.12	0.13	0.13	0.20	0.07	0.18	0.13
MgO	41.33	38.85	39.98	38.87	41.45	42.22	33.59	38.37	44.70	42.52
CaO	2.52	2.99	2.96	3.37	2.24	2.05	5.27	3.82	1.18	2.13
Na_2O	0.33	0.44	0.28	0.32	0.42	0.29	0.66	0.44	0.17	0.37
K_2O	0.03	0.01	0.05	0.03	0.02	0.00	0.00	0.03	0.04	0.04
P_2O_5	0.04	0.04	0.05	0.04	0.05	0.02	0.13	0.07	0.01	0.04
Total	101.18	100.93	99.64	100.45	100.73	99.83	101.79	100.83	100.46	100.17
Mg#	0.90	0.89	0.91	0.89	0.89	0.91	0.86	0.89	0.91	0.91

Sample rock name location texture	KB4 Sp-Lh PT PO	KB41 Sp-Ha PT PO	KB18 Sp-Lh PT EQ	KB35 Sp-Ha PT EQ	ADTM109 Host rock AD	EBBM1-47 Host rock EB	KB167 Host rock PT	KB168 Host rock PT
SiO_2	44.37	44.13	44.49	45.61	43.06	48.29	46.60	45.48
TiO_2	0.13	0.15	0.11	0.12	2.85	1.82	2.11	1.99
Al_2O_3	4.66	4.25	4.12	4.11	10.67	16.63	14.27	14.84
FeO	8.66	8.51	8.18	10.02	14.40	10.22	11.37	11.32
MnO	0.09	0.19	0.12	0.21	0.25	0.27	0.19	0.17
MgO	37.28	40.54	40.32	37.95	14.93	7.91	10.32	11.77
CaO	2.96	2.61	2.55	3.05	10.00	8.62	9.07	10.55
Na_2O	2.12	0.44	0.38	0.27	2.50	3.47	3.31	2.35
K_2O	0.05	0.04	0.01	0.02	0.52	0.80	1.32	1.19
P_2O_5	0.03	0.07	0.01	0.03	0.21	0.42	0.19	0.34
Total	100.35	100.93	100.29	101.39	99.40	98.45	98.74	100.00
Mg#	0.88	0.89	0.90	0.87	0.65	0.58	0.62	0.65

AD Adam's Diggings, *EB* Elephant Butte, *PT* Potrillo, *Sp-Lh* spinel lherzolite, *Sp-Ha* spinel harzburgite, *PR* protogranular, *PO* porphyroclastic, *EQ* equigranular

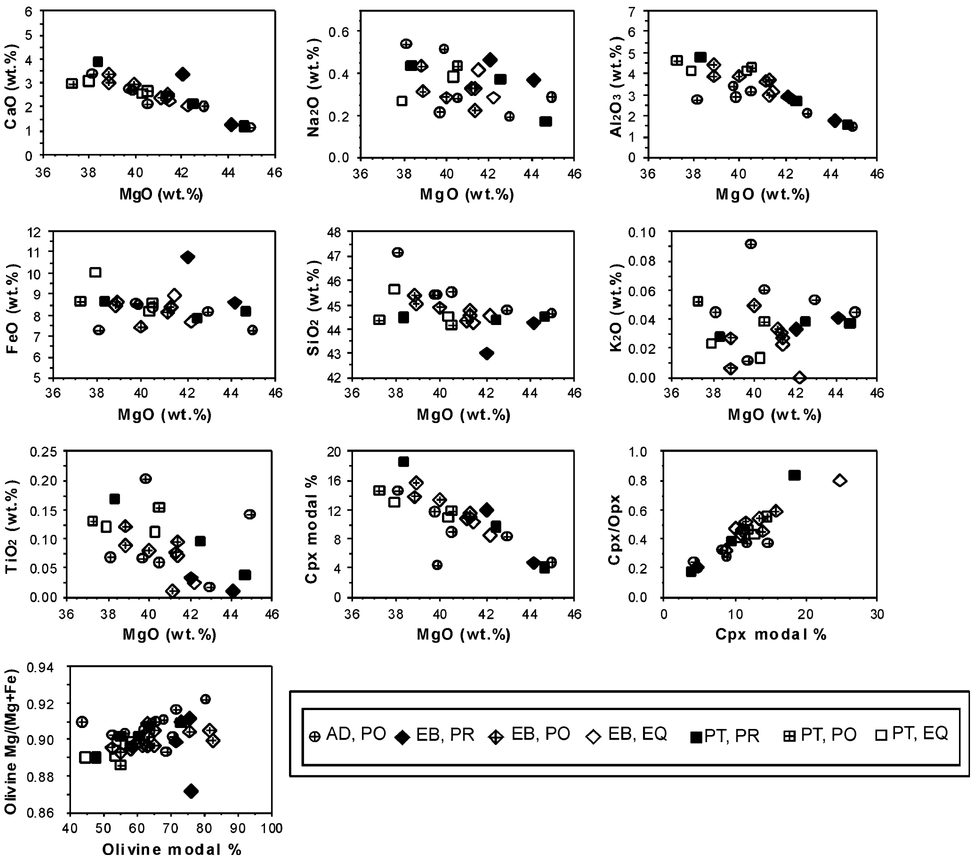

Fig. 2 Whole-rock oxides and modal clinopyroxene (Cpx) versus MgO, modal clinopyroxene versus modal Cpx/Opx ratio, and modal olivine versus olivine Mg/(Mg+Fe) for spinel peridotites. *AD* Adam's Diggings, *EB* Elephant Butte, *PT* Potrillo, *PR* protogranular, *PO* porphyroclastic, *EQ* equigranular

aration of the glass bead at 1,100°C, or metasomatic processes (Xu et al. 2000). Clinopyroxene modal percentage also decreases with increasing MgO content. This reduction, coupled with CaO and Al_2O_3 contents of spinel lherzolites from the three sites that are generally less than 3 wt% and 3.5 wt%, respectively, suggests that the upper mantle under these xenolith locations has undergone one or more depletion events.

Primitive mantle-normalized REE patterns for spinel peridotites from the rift shoulder (Adam's Diggings) display LREE enrichment (Fig. 3a) and those from the rift axis (Elephant Butte and Potrillo) display mostly flat and LREE-depleted patterns (Fig. 3b, c). Different textural types do not display significantly different patterns in the Potrillo samples, but undeformed rocks (protogranular texture) from Elephant Butte are more enriched in LREE than deformed rocks (porphyroclastic and equigranular textures. The host rocks from the three sites display very similar normalized REE patterns.

Trace elements in clinopyroxenes

Trace element and REE compositions of clinopyroxenes are summarized in Table 2. Trace elements prefer the larger sites of clinopyroxene relative to the octahedral sites of orthopyroxene, olivine, and spinel, thus clinopyroxenes are the main carriers of REE, Ti, and Zr in spinel peridotite (Nagasawa et al. 1980; Stosch 1982). Typically, abundances of these elements decrease in the order clinopyroxene > orthopyroxene > olivine > spinel. All spinel peridotite xenoliths from Adam's Diggings are characterized by porphyroclastic textures and clinopyroxenes are strongly enriched in LREE (Fig. 4).

REE compositions of clinopyroxenes are used to recognize metasomatism affecting spinel peridotites from the rift axis (Elephant Butte and Potrillo) as shown in Fig. 5. For xenoliths from Elephant Butte (Fig. 5a), primitive mantle-normalized clinopyroxene $(La/Yb)_n$ ratios progressively increase with increasing depth of xenolith equilibration. Among the three texture types, xenoliths with protogranular texture display the highest LREE/HREE ratios and appear to be the only spinel peridotites at this location to have undergone metasomatic enrichment (Fig. 5c). Deformed spinel peridotites (porphyroclastic and equigranular), with low LREE/HREE ratios, are interpreted as having undergone melt extraction without subsequent metasomatism (Fig. 5c). For xenoliths from Potrillo,

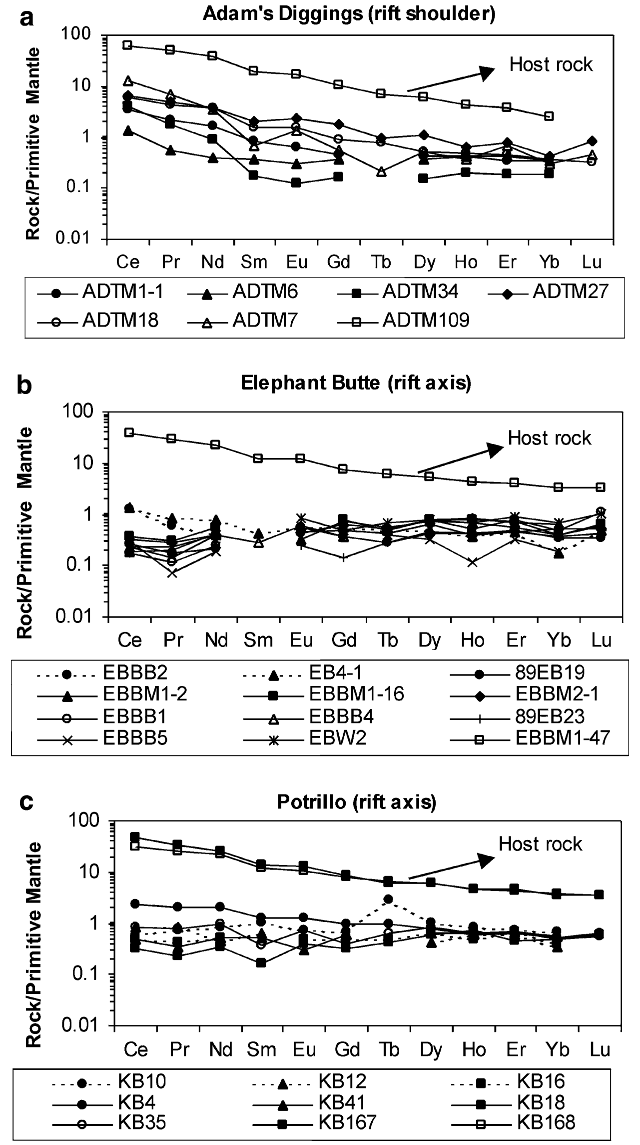

Fig. 3 **a–c** Primitive mantle-normalized REE abundances for spinel peridotite xenoliths and host rocks from **a** Adam's Diggings, **b** Elephant Butte, and **c** Potrillo. Primitive values are from Hofmann (1988). ADTM109, EBBM1-47, KB167, and KB168 are host rocks. *Dot lines* are undeformed rocks (protogranular texture), and *solid lines* are deformed rocks (porphyroclastic and equigranular textures)

the primitive mantle-normalized clinopyroxene (La/Yb)$_n$ ratio does not increase with depth indicating that metasomatism is not related to textural type (Fig. 5b). Chondrite-normalized LREE compositions of clinopyroxene are variably enriched or depleted, and also do not systematically correlate with xenolith textural type (Fig. 5d). Roden and Shimizu (1993) recognized similarly variable REE compositions for clinopyroxene in spinel peridotite xenoliths from both Colorado Plateau and Basin and Range locations. They interpreted LREE-depleted clinopyroxenes to be residues of partial melting and LREE-enrichment to be the product of interaction with alkaline magmas or metasomatic fluids.

Xenolith depletion by melt extraction

Partial melting and extraction of basaltic components from the mantle has likely occurred multiple times, resulting in chemical depletion of the upper mantle. Roden et al. (1988) argued that spinel lherzolite at Kilbourne Hole (Potrillo) differentiated from the primitive mantle as much as 1 billion years ago. Volcanic activity related to the Oligocene to Recent evolution of the Rio Grande rift has continued this depletion process. Therefore, mantle depletion by melt extraction as discussed below includes both pre- and syn-rifting events.

Whole-rock and mineral chemical compositions and mineral modes document this depletion process. Evidence of depletion includes decreasing bulk rock CaO, Al_2O_3, and TiO_2 contents, and decreasing clinopyroxene modal percentages with increasing MgO (Fig. 2). Clinopyroxene/orthopyroxene ratios decrease with decreasing clinopyroxene abundance (Fig. 2), which indicates that the depletion process involved partial melting, because clinopyroxene is the principal mineral consumed during partial melting of spinel lherzolites to produce basaltic magmas. Olivine modal percentages increase with melt extraction and Mg is more enriched than Fe in residual olivine and other major minerals in spinel lherzolite because Fe is relatively incompatible. Therefore, increasing olivine modal percentages with increasing olivine Mg/(Mg + Fe) is strong evidence of mantle depletion (Fig. 2).

Recognizing that clinopyroxene dominates bulk distribution coefficients for incompatible elements in spinel peridotite, the rare earth elements in clinopyroxene can be used to model batch and fractional melting. The equations for batch melting and fractional melting are

$$C_{cpx}/C_o = D_{cpx}/\left[D_{cpx} \times X_{cpx} \times (1-F)+F\right] \qquad (1)$$

and

$$C_{cpx}/C_o = (1-F)^{(1/D_{cpx}\times X_{cpx})-1}, \qquad (2)$$

respectively (Norman 1998), where C_{cpx} is the concentration of an element in residual clinopyroxene, C_o is the concentration of the element in the initial bulk composition of the source, assumed to be the compo-

Table 2 Trace and rare earth element analyses (ppm) of clinopyroxene from Rio Grande rift xenoliths

Sample rock	AD1-1	AD1-2	ADTM6	ADTM7	ADTM8	ADTM10	ADTM12	ADTM13	ADTM18	ADTM27	ADTM34
name location	Sp-Lh	Sp-Lh	Sp-Lh	Sp-Lh	Sp-Lh	Sp-Lh	Sp-Lh	Sp-Lh	Sp-Ha	Sp-Ha	Sp-Lh
texture	AD PO	AD PO	AD PO	AD PO	AD PO	AD PO	AD PO	AD PO	AD PO	AD PO	AD PO
Sr	268.6	229.7	116.3	397.8	221.8	122.4	424.7	389.6	522.4	305.9	636.4
Y	6.0	4.7	8.9	6.8	7.9	4.9	8.9	8.3	23.0	12.8	5.0
Zr	3.8	3.1	13.6	3.8	2.2	1.8	26.4	39.1	97.5	75.9	3.8
La	13.7	10.5	9.3	22.0	11.6	5.3	13.4	15.9	35.1	12.1	26.4
Ce	39.9	26.2	14.8	31.4	25.6	6.8	55.4	54.8	92.4	45.0	54.2
Pr	3.4	2.3	1.3	2.3	2.6	0.5	6.6	6.5	13.9	5.4	4.7
Nd	10.4	6.3	3.6	5.2	8.1	1.6	24.9	20.8	65.0	22.1	11.3
Sm	1.2	1.1	0.9	0.7	0.7	0.3	3.8	3.5	10.3	3.6	1.0
Eu	0.3	0.3	0.3	0.3	0.3	0.1	1.1	1.0	3.0	1.4	0.3
Gd	0.7	0.7	1.1	1.0	0.5	0.5	2.2	1.8	8.4	3.4	0.7
Tb	0.2	0.1	0.3	0.2	0.2	0.1	0.3	0.3	1.1	0.5	0.2
Dy	1.2	0.5	1.6	1.5	1.3	0.9	1.9	1.6	5.3	2.8	1.0
Ho	0.3	0.2	0.4	0.2	0.3	0.3	0.4	0.4	1.0	0.5	0.2
Er	0.7	0.6	1.4	1.0	1.0	0.9	1.3	0.9	2.6	1.6	0.8
Tm	0.1	0.0	0.2	0.2	0.1	0.1	0.1	0.1	0.3	0.2	0.1
Yb	0.6	0.5	1.2	0.8	1.0	0.9	0.9	0.8	1.7	0.9	0.8
Lu	0.1	n.d.	0.1	0.1	0.2	0.1	0.1	0.2	0.3	0.2	0.1
Hf	n.d.	n.d.	0.3	n.d.	0.1	0.2	0.1	0.3	1.6	1.7	n.d.

Sample rock	ADTM37	89EB18	EBBB2	EB4-1	EB6-4	89EB17	89EB19	89EB24	90EB1	EBBM1-2	EBBM1-16
name location	Sp-Ha	Sp-Lh	Sp-Ha	Sp-Lh	Sp-Ha	Sp-Lh	Sp-Lh	Sp-Lh	Sp-Ha	Sp-Lh	Sp-Lh
texture	AD PO	EB PR	EB PR	EB PR	EB PR	EB PO	EB PO	EB PO	EB PO	EB PO	EB PO
Sr	467.0	26.9	196.7	95.4	67.7	32.7	16.8	33.8	51.7	19.1	52.6
Y	22.3	6.0	2.4	12.4	14.9	17.0	14.6	16.1	15.7	13.7	15.9
Zr	273.8	15.4	31.8	19.4	28.8	19.0	11.9	18.6	20.6	12.2	23.9
La	19.7	0.4	7.4	3.4	1.1	0.2	0.1	0.2	0.6	0.1	0.4
Ce	63.8	2.1	12.9	7.5	4.5	1.5	0.8	1.5	2.2	1.0	2.5
Pr	8.1	0.4	1.6	1.0	0.9	0.5	0.4	0.5	0.5	0.3	0.7
Nd	36.8	3.2	7.6	5.6	6.1	4.1	2.1	4.0	3.6	3.2	4.7
Sm	8.7	1.1	n.d.	1.5	1.8	1.5	1.1	1.4	1.5	1.1	1.7
Eu	2.8	0.4	0.4	0.6	0.6	0.7	0.5	0.7	0.7	0.4	0.5
Gd	6.1	1.7	n.d.	2.0	2.5	2.6	1.9	2.2	2.2	1.9	2.5
Tb	1.0	0.3	n.d.	0.5	0.5	0.4	0.4	0.5	0.5	0.4	0.5
Dy	4.6	1.5	n.d.	2.4	3.3	3.8	3.0	3.9	3.5	2.9	3.6
Ho	1.0	0.3	0.2	0.5	0.7	0.7	0.7	0.6	0.7	0.5	0.8
Er	2.7	0.9	0.4	1.5	2.1	2.3	2.2	2.5	2.3	2.0	2.3
Tm	0.4	0.1	n.d.	0.2	0.3	0.3	0.3	0.3	0.3	0.2	0.3
Yb	1.4	0.5	0.5	1.1	1.6	1.7	1.6	1.7	1.7	1.7	1.9
Lu	0.1	0.1	0.1	0.2	0.3	0.2	0.3	0.4	0.3	0.2	0.3
Hf	3.6	0.5	0.8	0.5	1.0	1.0	0.5	0.8	0.7	0.2	0.8

Sample rock	EBBM2-1	EBBB1	EBBB4	EBBB5	EB6-2RI	EBW-1	EBW-2	KB3	KB10	KB12	KB16
name location	Sp-Lh	Sp-Lh	Sp-Lh	Sp-Lh	Sp-Ha	Sp-Ha	Sp-Lh	Sp-Lh	Sp-Lh	Sp-Ha	Sp-Lh
texture	EB PO	EB PO	EB PO	EB EQ	EB EQ	EB EQ	EB EQ	PT PR	PT PR	PT PR	PT PR
Sr	61.7	20.2	36.4	2.6	51.1	29.6	19.7	34.2	48.0	124.4	74.4
Y	16.9	15.6	17.2	14.1	11.1	14.7	20.9	16.5	14.3	3.2	13.7
Zr	28.8	15.1	19.3	4.8	16.4	15.1	12.5	17.0	21.1	11.1	25.6
La	0.5	n.d.	0.2	0.1	0.5	0.3	0.2	1.1	0.8	4.7	0.9
Ce	3.3	1.0	1.0	0.4	3.0	1.5	0.5	2.5	3.5	9.3	3.5
Pr	0.8	0.2	0.3	n.d.	0.5	0.5	0.2	0.6	0.8	1.2	0.8
Nd	5.6	3.6	2.8	1.8	3.6	3.2	3.9	3.3	6.0	3.1	4.6
Sm	1.8	1.3	1.3	0.9	1.2	1.1	1.0	1.4	1.9	1.2	1.6
Eu	0.7	0.6	0.7	0.3	0.6	0.5	0.8	0.6	0.6	0.3	0.6
Gd	2.4	2.5	2.4	1.5	1.6	2.5	1.7	2.3	2.8	n.d.	2.2
Tb	0.6	0.2	0.5	0.4	0.3	0.4	0.7	0.4	0.6	0.2	0.5
Dy	3.2	2.3	3.1	3.1	2.3	3.0	2.1	3.3	2.9	0.6	3.1
Ho	0.8	0.8	0.8	0.7	0.5	0.6	0.8	0.6	0.6	0.2	0.6
Er	2.4	1.5	2.4	2.2	1.3	2.2	3.4	2.2	2.5	n.d.	2.1
Tm	0.3	0.2	0.4	0.2	0.2	0.4	0.3	0.4	0.3	n.d.	0.3

Table 2 continued

Sample rock name location texture	EBBM2-1 Sp-Lh EB PO	EBBB1 Sp-Lh EB PO	EBBB4 Sp-Lh EB PO	EBBB5 Sp-Lh EB EQ	EB6-2RI Sp-Ha EB EQ	EBW-1 Sp-Ha EB EQ	EBW-2 Sp-Lh EB EQ	KB3 Sp-Lh PT PR	KB10 Sp-Lh PT PR	KB12 Sp-Ha PT PR	KB16 Sp-Lh PT PR
Yb	1.9	2.3	1.7	1.5	1.3	2.1	2.8	2.1	1.5	0.4	1.2
Lu	0.3	0.1	0.3	0.4	0.2	0.2	0.4	0.3	0.3	0.1	0.2
Hf	0.9	0.4	0.6	0.4	0.6	0.5	0.8	0.6	0.7	0.5	0.8

Sample rock name location texture	KB25 Sp-Lh PT PR	KB57 Sp-Lh PT PR	KB4 Sp-Lh PT PO	KB14 Sp-Lh PT PO	KB41 Sp-Lh PT PO	KB52 Sp-Lh PT PO	KB18 Sp-Lh PT EQ	KB35 Sp-Lh PT EQ	KB56 Sp-Ha PT EQ
Sr	54.0	34.3	125.1	37.4	29.2	88.0	27.9	71.9	39.6
Y	15.9	9.1	16.5	15.5	14.0	13.9	15.3	12.1	14.4
Zr	23.5	7.5	28.3	18.3	14.9	16.2	13.0	15.7	24.0
La	0.6	0.8	3.6	0.4	0.2	2.7	0.5	2.2	1.2
Ce	3.1	3.3	17.8	n.d.	1.5	9.7	1.8	11.1	5.6
Pr	0.8	0.5	3.5	0.5	0.4	1.5	0.5	1.6	1.1
Nd	5.3	3.0	20.1	3.8	3.8	7.5	3.9	7.3	7.2
Sm	1.8	0.9	5.0	1.2	1.5	1.5	1.4	1.8	1.8
Eu	0.7	0.4	1.4	0.7	0.6	0.8	0.7	0.8	0.7
Gd	2.4	1.6	4.1	2.1	2.0	1.9	2.7	1.9	2.9
Tb	0.5	0.3	0.6	0.5	0.5	0.5	0.5	0.4	0.5
Dy	3.5	2.1	4.2	3.6	2.4	2.7	3.3	2.2	3.0
Ho	0.7	0.3	0.7	0.6	0.6	0.7	0.7	0.5	0.6
Er	2.3	1.5	2.3	2.2	2.2	2.1	2.2	1.7	2.1
Tm	0.3	0.2	0.3	0.3	0.3	0.3	0.3	0.2	0.3
Yb	1.6	1.1	2.0	1.7	1.9	1.8	1.5	1.2	2.0
Lu	0.3	0.2	0.3	0.3	0.3	0.4	0.2	0.2	0.3
Hf	0.8	0.5	1.3	0.8	0.5	0.8	0.7	0.6	1.2

AD Adam's Diggings, *EB* Elephant Butte, *PT* Potrillo, *Sp-Lh* spinel lherzolite, *Sp-Ha* spinel harzburgite, *PR* protogranular, *PO* porphyroclastic, *EQ* equigranular

sition of the mantle before the continental crust formed (primitive mantle value; Hofmann 1988), D_{cpx} is the distribution coefficient for the element between clinopyroxene and basaltic melt (Kelemen et al. 1993; Halliday et al. 1995), X_{cpx} is the fraction of clinopyroxene in primitive mantle spinel peridotite (assumed to be 0.2; Fig. 2), and F is the weight fraction of melt produced. The assumption of C_o to be that of primitive mantle is reasonable but not unique, given the long, complex, and unknown history of the upper mantle. Accordingly, the results of the melting models are illustrative but similarly non-unique.

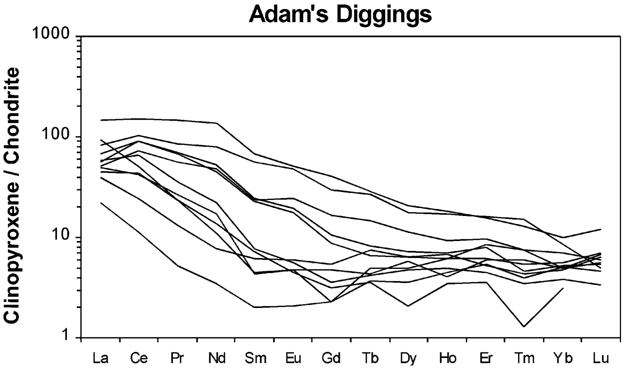

Fig. 4 Chondrite-normalized REE compositions for clinopyroxenes from Adam's Diggings' spinel peridotites. Chondrite values are from Sun and McDonough (1989)

Rift shoulder (Adam's Diggings)

Normalized whole-rock and clinopyroxene REE compositions for Adam's Diggings spinel lherzolites (Figs. 3, 4, respectively) are characterized by LREE enrichments, suggestive of mantle metasomatism (discussed later) following melt extraction. This argument follows from comparison of observed clinopyroxene incompatible element compositions with those predicted for residual clinopyroxene following batch or fractional melting (Fig. 6). Either of these melting processes would result in clinopyroxene having pronounced depletions in most incompatible elements, although fractional melting would be more efficient than batch melting in removing the most incompatible elements. Consequently, less incompatible elements, Y and Yb, were used to determine the degree of partial melting and to distinguish between batch melting and

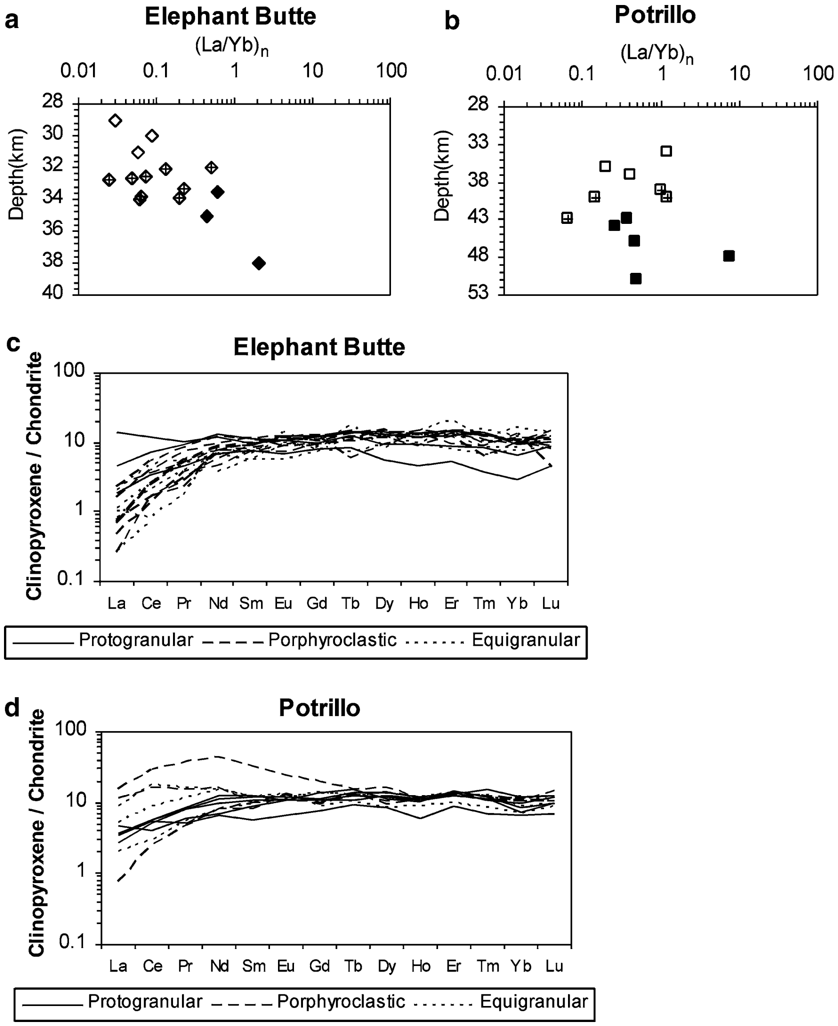

Fig. 5 **a–d** Primitive mantle-normalized $(La/Yb)_n$ versus depth (km) for clinopyroxenes from **a** Elephant Butte spinel peridotites and **b** Potrillo spinel peridotites. Chondrite-normalized REE compositions for clinopyroxenes from **c** Elephant Butte spinel peridotites and **d** Potrillo spinel peridotites. Xenolith extraction depths are from Kil and Wendlandt (2004). Symbols are as summarized in Fig. 2

fractional melting processes. As shown in Fig. 7a, b, the batch-melting model requires unreasonably high amounts of partial melting, up to and exceeding 30% (e.g., McKenzie 1985; McKenzie and O'Nions 1991), to explain the observed Y and Yb. By the same reasoning, spinel lherzolites from Adam's Diggings could have undergone 7–14% fractional melting. Phlogopite-bearing spinel harzburgites (ADTM18, ADTM27 and ADTM 37) are strongly REE-enriched, including Y and Yb (Fig. 7a, b), and could not be used to constrain the degree of partial melting.

Rift axis (Elephant Butte and Potrillo)

In contrast to Adam's Diggings, xenoliths from Elephant Butte and Potrillo are not noticeably enriched in LREE (Fig. 3), however clinopyroxene in protogranular textured xenoliths from Elephant Butte and in occasional xenoliths from all three texture groups at Potrillo show elevated LREE (Fig. 5). These observations are consistent with the results of batch and fractional melting models based on $(La/Yb)_n$ versus Lan contents of clinopyroxenes from these two locations (Fig. 7c, e). Recognizing that these simple models can only approximate complex chemical relations resulting from melting (perhaps occurring multiple times) and provide very qualitative explanations of melting processes, fractional melting models best describe the data, particularly those samples having low $(La/Yb)_n$ or requiring excessively large degrees of batch melting. Samples of undeformed (protogranular texture) rocks from Elephant Butte and occasional samples representing all texture types from Potrillo (Fig. 7c, e, respectively) deviate from fractional melting models [higher $(La/Yb)_n$] due to LREE enrichment, as noted above.

Only Y and Yb were used to determine the degree of partial melting for comparison with Adam's Diggings (Fig. 7d, f). Fractional melting calculations show that most spinel peridotites from both rift axis loca-

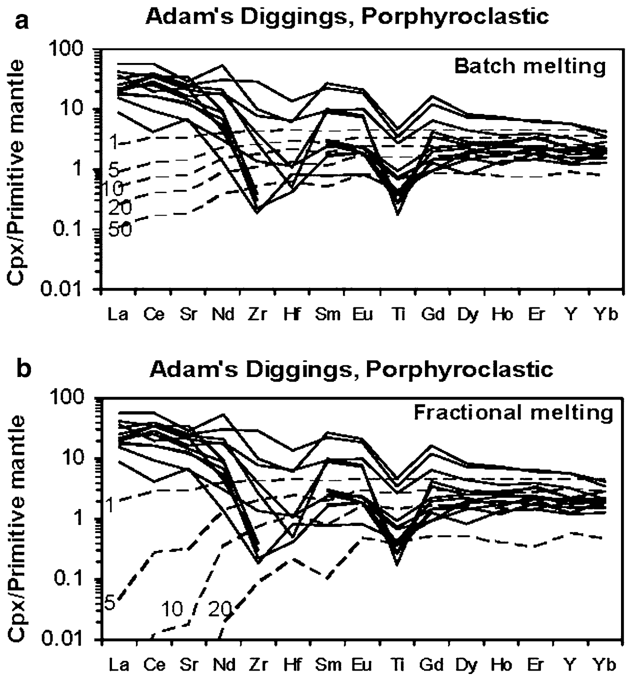

Fig. 6 **a–b** Comparison of trace element compositions predicted for residual clinopyroxene having undergone partial melting (*dash lines*) with analyzed primitive mantle-normalized clinopyroxene compositions (*solid lines*): **a** batch melting (1, 5, 10, 20, and 50%; *dashed lines*), and **b** fractional melting (1, 5, 10, and 20%; *dashed lines*)

tions have undergone <5% melting, although the total range of fractional melting at Potrillo and Elephant Butte is similar to that for Adam's Diggings. Undeformed (protogranular) and deformed (porphyroclastic and equigranular) rocks from Elephant Butte are characterized by similar ranges of fractional melting. Deformed (equigranular and porphyroclastic texture) spinel peridotites from Potrillo are characterized by significantly less fractional melting (2–5%) than undeformed xenoliths (up to 16%). This difference may reflect undeformed xenoliths being derived from greater depths and higher temperatures (and higher recrystallization rates) than deformed rocks (Kil and Wendlandt 2004). Thus, even though the current surface expression of volcanic materials is greater along the rift axis than on the rift shoulder, calculations suggest comparable amounts of melting for the two regions. The range of melting, however, may be more restricted for rift shoulder (Adam's Diggings) xenoliths and lower degrees of fractional melting are indicated for deformed peridotites from Potrillo. These results are consistent with models that upper mantle depletion started prior to rifting in the Proterozoic and that the upper mantle under the Rio Grande rift has undergone multiple extraction events from the primitive mantle.

Xenolith enrichment by mantle metasomatism

Mantle metasomatism generally refers to an enrichment process involving incompatible elements, e.g., K, Rb, Sr, Ba, LREE, Ti, Nb, Zr, P, U, and Th (Roden and Murthy 1985). Mantle metasomatism can be subdivided into two types (Dawson 1984): (1) patent metasomatism (modal metasomatism) is characterized by mineralogical changes, including introduction of hydrous (amphibole, phlogopite) and/or anhydrous minerals (zircon, apatite, rutile, crichtonite-series minerals); and (2) cryptic metasomatism is characterized by compositional enrichment without the introduction of new minerals. A useful, but not exact, indicator of cryptic metasomatism for the Rio Grande rift occurrences is xenoliths or mantle clinopyroxenes having normalized $(La/Yb)_n > 1$. Spinel peridotites from Adam's Diggings display both patent and cryptic metasomatism, and those from Elephant Butte and Potrillo (rift axis) display only cryptic metasomatism.

Metasomatic agent

Metasomatic agents in the upper mantle are generally considered to be of three types: silicate magma, carbonatite magma, and H_2O–CO_2 fluid. Carbonatite metasomatism characteristically results in distinctive petrographic, whole rock, and trace element geochemical changes primarily involving clinopyroxene (Yaxley et al. 1991; Roden and Shimizu 1993). Wehrlite xenoliths, produced by interaction between carbonatite magma and upper mantle lithologies, have not been reported from the Rio Grande rift, and there are no known carbonatite occurrences in the Rio Grande rift (Yaxley et al. 1991; Roden et al. 1988; Baldridge 1979). Accordingly, CaO/Al_2O_3 ratios of spinel peridotites from the three sites are generally characterized by lower CaO/Al_2O_3 ratios than wehrlites (Yaxley et al. 1991). Carbonatites have significantly lower Ti/Eu than primitive mantle values (Hofmann 1988), yet Ti/Eu in lherzolite from the three sites are greater than the primitive mantle values (Fig. 8). Because partial melting does not change Ti/Eu whole-rock compositions, these Ti/Eu suggest that metasomatism agents in the upper mantle under the Rio Grande rift are not likely to include carbonatitic magma.

Wyllie (1977) and Menzies et al. (1985) have argued that large amounts of CO_2 can be released by basaltic and other alkalic magmas at low pressure. CO_2-rich fluids associated with silicate melts have been shown to strongly fractionate LREE (Wendlandt and Harrison 1979), suggesting a mechanism for LREE enrichment

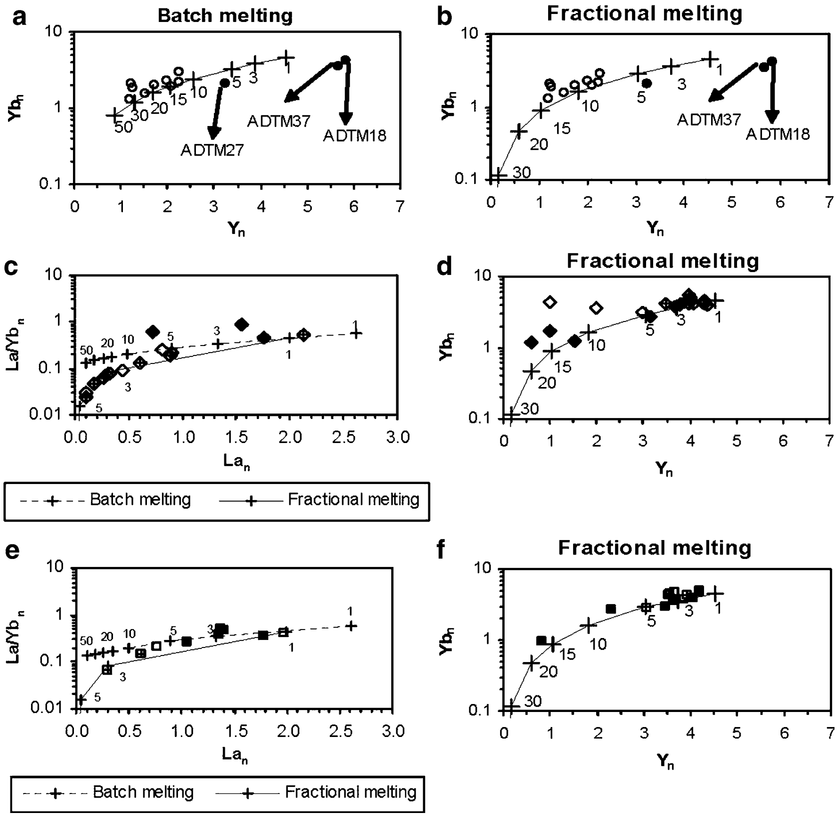

Fig. 7 **a–f** Comparison of partial melting models for Y_n and Yb_n contents of clinopyroxene in spinel peridotites from Adam's Diggings: **a** batch melting (between 1 and 50%) and **b** fractional melting (between 1 and 30%). Primitive mantle values are from Hofmann (1988). *Open circles* are for Cpx from spinel lherzolites and *closed circles* (ADTM18, ADTM27, and ADTM37) are for Cpx from phlogopite-bearing spinel harzburgite. Spinel harzburgites could not be used to determine the degree of melting because of metasomatic modification. Comparison of partial melting models for La_n and $(La/Yb)_n$ contents of clinopyroxene in spinel peridotites from **c** Elephant Butte and **e** Potrillo. *Dash line* indicates batch melting (1–50%) and *solid line* indicates fractional melting (1–5%). Strongly LREE-enriched protogranular rocks show a deviation from the fractional melting line. Comparison of fractional melting models for Y_n and Yb_n contents of clinopyroxene in spinel peridotites from **d** Elephant Butte, and **f** Potrillo. Symbols for Fig. 6c, d, e, f are as summarized in Fig. 2

by CO_2-rich fluids. However, Hamilton et al. (1989) suggest the alternative interpretation that REE are preferentially partitioned into the silicate melt. Also, Menzies and Hawkesworth (1987) suggest that melt is a more efficient metasomatic agent than fluids, because the high reactivity of H_2O–CO_2 fluids in hydration and carbonation reactions and partial melting limits fluid mobility. For these reasons, therefore, metasomatic agents in the upper mantle under the Rio Grande rift are likely to be silicate magma rather than fluids and carbonatite magma.

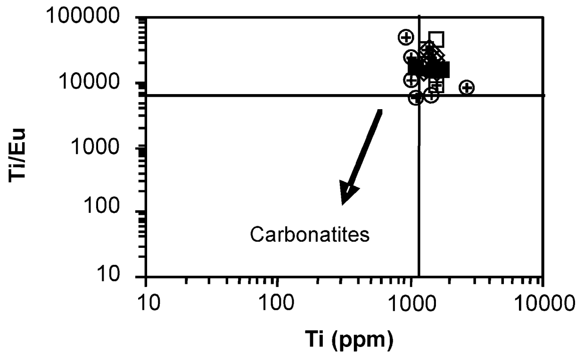

Fig. 8 Log Ti (ppm) versus Ti/Eu for spinel peridotites from the three localities. The *lines* indicate primitive mantle values for Ti and Ti/Eu from Hofmann (1988). Symbols are as summarized in Fig. 2

Elephant Butte and Potrillo

Assuming that metasomatic enrichment was caused by entrapment of metasomatizing silicate melt reacting with primary peridotite minerals, trace element distribution coefficients between xenolith clinopyroxene and silicate melt can be used to identify compositional attributes of the metasomatic agent. Concentrations of components in the hypothetical silicate melt metasomatic agent are determined using the following equation:

$$C_{\text{silicate melt}} = C_{\text{cpx}}/D_{\text{cpx/silicate melt}}, \tag{3}$$

where $C_{\text{silicate melt}}$ and C_{cpx} are concentrations of an element in the hypothetical silicate melt and clinopyroxene, and $D_{\text{cpx/silicate melt}}$ is the distribution coefficient for an element between clinopyroxene and silicate melt.

Calculated silicate melt compositions for the protogranular texture rocks at Elephant Butte utilize distribution coefficients between clinopyroxene and alkali basalt melt ($D_{\text{cpx/alkali basalt melt}}$) because the host rock of Elephant Butte is alkali basalt. D (distribution coefficient) values are influenced by pressure, temperature, and phase compositions, therefore, the calculations used $D_{\text{cpx/alkali basalt melt}}$ values from Nicholls and Harris (1980) which were determined for upper mantle conditions of 1,080°C and 15 kb. Values of C_{Cpx} used in Eq. 1 were obtained by LA-ICPMS analysis as part of this research. Subsequently, hypothetical (calculated) silicate melt compositions were compared to actual host rock analyses (alkali basalt) to test whether the metasomatism source for protogranular spinel peridotites could be alkali basalt melt. In Fig. 9a, the calculated hypothetical silicate melt composition compares well with the host rock composition (alkali basalt). Beccaluva et al. (2001) suggested that complete chemical rehomogenization of a 1 mm clinopyroxene requires a time span of 4.8–16 ka, based on diffusion models for clinopyroxene. Therefore, the metasomatic agent for protogranular rocks at Elephant Butte could have been similar to the host rock melt and may be related to this melt or to earlier alkali basaltic magmatism. As shown in Fig. 5a, primitive mantle-normalized clinopyroxene $(\text{La/Yb})_n$ ratios increase with increasing depth of equilibration for Elephant Butte xenoliths. This trend suggests that the protogranular texture xenoliths at this location experienced metasomatic enrichment (Fig. 5a) whereas xenoliths with deformed texture (porphyroclastic and equigranular) have undergone melt extraction without subsequent metasomatism (Fig. 5a, c).

Hypothetical silicate melt calculations for Potrillo xenoliths (Fig. 9b, c), again using $D_{\text{Cpx/Alkali basalt melt}}$

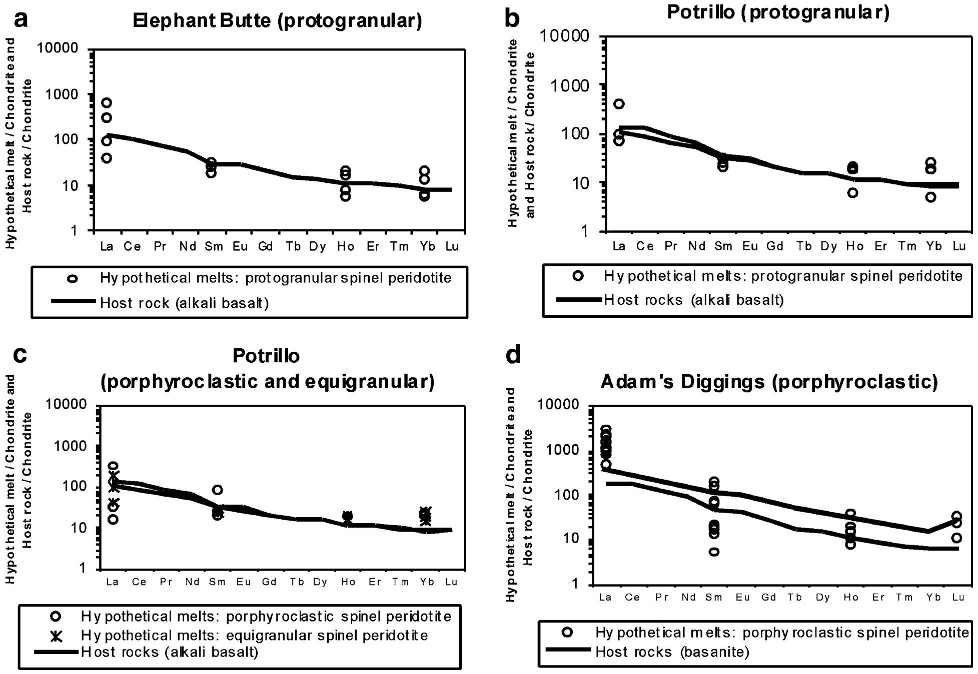

Fig. 9 **a–d** Comparison of REE compositions for hypothetical melt (symbols) and alkali basalt host rock for **a** Elephant Butte spinel peridotites with protogranular texture, **b** Potrillo protogranular spinel peridotites, and **c** Potrillo porphyroclastic and equigranular spinel peridotites. $D_{\text{Cpx/Alkali basalt melt}}$ at 1,080°C and 15 kb from Nicholls and Harris (1980) were used to calculate the hypothetical melts for Elephant Butte and Potrillo spinel peridotites. **d** Comparison of REE compositions for hypothetical melt (symbol) and basanite host rock compositions (this study and sample Z6.6.12(2) of Baldridge et al., 1991) for Adam's Diggings spinel peridotites. $D_{\text{Cpx/Basanite melt}}$ at 1050°C and 15 kb from Adam and Green (1994) were used to calculate the hypothetical melts for Adam's Diggings spinel peridotites. Chondrite values are from Sun and McDonough (1989). Host rock data are from Kil (2002)

values for conditions of 1,080°C and 15 kb (Nicholls and Harris 1980), support the conclusion that all three textural types at this location have undergone metasomatism by the host rock melt and/or alkali basaltic magmatism preceding the entrainment of mantle xenoliths by the host magma. This conclusion is based on the similarity of the calculated hypothetical silicate melt composition with the host rock composition (alkali basalt). Metasomatism in xenoliths from Potrillo is not related to textural type (Fig. 5b, d).

Adam's Diggings

The hypothetical silicate melt at Adam's Diggings was calculated using distribution coefficients between clinopyroxene and basanite ($D_{\mathrm{cpx/basanite\ melt}}$) from Adam and Green (1994), which were determined for upper mantle conditions of 1,050°C and 15 kb. In Fig. 9d, compositions of chondrite-normalized hypothetical silicate melts derived for xenolith clinopyroxene using (Eq. 3), agree with host rock compositions (basanite) for HREE, but display much higher LREE than the host rocks. The HREE signatures for these harzburgites (Fig. 9d) may be explained by enrichment processes involving the host rock or unrecognized earlier basanitic magmatism. The enriched LREE signatures, however, require an additional or alternative enrichment event.

Early cryptic metasomatism

A possible source for the early LREE-enrichment is melt derived from small degrees of partial melting of pyroxene- and phlogopite-bearing peridotite (e.g., Carlson and Nowell 2001), perhaps associated with the period of extensive volcanic activity that occurred from approximately 37 to 20 Ma in or near the Rio Grande rift. Minette magmas, derived by melting of phlogopite-bearing mantle, formed shallow intrusives on the Colorado Plateau at this time (Vaniman et al. 1985) and may be related to the early metasomatism recorded in the Adam's Diggings xenoliths. One manifestation of this early igneous activity occurred at approximately 25–30 Ma at Cerros de las Mujeres, New Mexico, located 25 km northwest of Adam's Diggings (Vaniman et al. 1985). The Cerros de las Mujeres minettes display very high chondrite-normalized La/Yb ratios (about 60; Vaniman et al. 1985) possibly related to small degrees of partial melting. Accordingly, REE enrichment in Adam's Diggings xenoliths could have been produced by interactions involving mantle and melts of this type.

Patent (modal) metasomatism

Phlogopites in xenoliths from Adam's Diggings are deformed and, thus, believed to have formed at some undetermined time prior to incorporation in host basalt. The introduction of phlogopite into spinel peridotites results from reaction between potassium-rich fluid or melt and magnesium-rich minerals within the phlogopite stability field (Sato et al. 1996). A possible source of potassium to form phlogopite at Adam's Diggings may be the subducted Farallon oceanic plate, which was overridden by the North American continent beginning approximately 140–100 Ma ago (late Jurassic and Cretaceous period) and continuing until about 50 Ma ago. Johnson et al. (1996) emphasized the importance of melt infiltration related to ancient subduction processes to explain the presence of hydrous phases in xenoliths from Cenozoic rifts. Alternatively, the metasomatic phlogopite may have been produced by the same minette metasomatic event that resulted in enrichment of clinopyroxene in LREE and other incompatible trace elements. A number of studies, however, have concluded that the appearance of phlogopite typically indicates a distinct metasomatic event from that resulting in LILE enrichment in clinopyroxene (Menzies et al. 1987; O'Reilly and Griffin 1988; Johnson et al. 1996). In the rift axis (Elephant Butte and Potrillo), phlogopite is absent because of the breakdown of phlogopite during rift-related partial melting or, alternatively, phlogopite was never present.

In summary, there may be as many as two or three metasomatic events at Adam's Diggings. The simplest explanation for the observed patent and cryptic metasomatism involves the interaction of xenolith mantle with deep-sourced potassic minette magmatism during early rifting. Alternatively, the patent metasomatism and the LREE enrichment of clinopyroxene may be decoupled and involve patent (modal) metasomatism before rifting caused by mixing MORB-type mantle and hydrous fluids from subducted slabs that were enriched in alkalis and LILE (old subducted slabs), followed by metasomatism involving a minette-type melt composition during early rifting (Oligocene). Whether or not this minette event was followed by metasomatism involving basanitic magmatism, similar in composition to the host rock, cannot be proven or dismissed.

Discussion (Upper mantle evolution)

A model for upper mantle (spinel lherzolite stability field) evolution under the southern Rio Grande rift axis and rift shoulder can be proposed that is based on interpretations of major and trace element whole-rock and mineral compositions. Particular emphasis is placed on types and distributions of texture types, pressure and temperature conditions of origin of xenoliths (Kil and Wendlandt 2004), and mantle depletion and enrichment events relative to the formation of the Rio Grande rift, i.e., prior to rifting (greater than 37 Ma), early rifting (Oligocene to middle Miocene; 37–15 Ma), and late rifting (middle Miocene to Holocene; 15–0 Ma). An assumption of this model is that there was no significant North American plate movement during the late rifting period, when xenoliths were transported to the surface.

Prior to rifting (greater than 37 Ma)

Chemical and isotope data for volcanic rocks and mantle xenoliths from southwestern USA, including the Rio Grande rift, indicate that the upper mantle was heterogeneous at this time with MORB-type and OIB-type (old subducted slab) mantle components (Frey and Prinz 1978; Roden et al. 1988; Menzies et al. 1987; Mattery et al. 1985; Kyser and Rison 1982; Leeman 1982). The timing of partial melting events is not well constrained but upper mantle under the Rio Grande rift has undergone multiple extraction events from more than 1 billion years (Roden et al. 1988) to present. The maximum degree of partial melting, indicated by less incompatible elements (e.g., Y and Yb) is comparable for the rift axis (Elephant Butte and Potrillo) and the rift shoulder (Adam's Diggings). However, along the rift axis, most spinel peridotites and, in particular, porphyroclastic and equigranular textured spinel peridotites apparently experienced smaller degrees of partial melting relative to rift shoulder peridotites. This difference may be a consequence of varying extraction depths for textural types from different locations.

From about 140 Ma years ago, the oceanic Farallon plate, coming from the west, subducted beneath the North American continental margin. During this period, the first enrichment process recognized in this study may have occurred (MM1 in Fig. 10a), involving the reaction of a potassium-enriched metasomatic agent (perhaps from an old subducted slab) with a depleted MORB-type mantle to produce phlogopite. The depth and lateral extent of this metasomatic event is not known, however, the recognition of subduction-related volcanism in the Rio Grande rift, southern New Mexico (McMillan et al. 2000), provides support for this metasomatic agent. Alternatively, this first enrichment process may be related to magmatic processes occurring during the early stage of rifting (as discussed previously).

Early rifting (Oligocene to middle Miocene; 37–15 Ma)

A clear explanation of the rifting mechanism for the Rio Grande rift, i.e., active or passive (Sengor and Burke 1978), has not been forthcoming. By whatever mechanism, however, the lithosphere was attenuated by asthenospheric upwelling during the Oligocene to middle Miocene (Fig. 10b). There are two magmatic pulses in the Rio Grande rift (Baldridge et al. 1980): an early pulse (late Oligocene–early Miocene) and a later episode (middle Miocene–Holocene). During the early pulse, magmatism associated with tectonic extension (rifting) began about 37 Ma, became widespread after 30 Ma, and waned from 20 to 15 Ma (Aldrich et al. 1986). Volcanic activity mainly occurred along the rift axis and 80% of all southern rift volcanics were erupted during this period (Bussod and Williams 1991). There are no known mantle xenolith suites in the central and southern part of the Rio Grande rift associated with volcanic activity during this period.

During rifting, deformation textures developed in the mantle under the Rio Grande rift. The brittle lithosphere was more easily deformed than the asthenosphere. The hotter and more attenuated mantle along the rift axis (Elephant Butte and Potrillo) produced three textural types. Heating promoted mineral growth (recrystallization), whereas extensive strain, related to asthenospheric upwelling, promoted mineral deformation. Therefore, the lowest temperature equigranular texture rocks (most deformed rocks) originated in the uppermost part of the lithosphere near the crust, whereas the highest temperature protogranular texture rocks (most recrystallized rocks) originated at greater depths. Intermediate temperature porphyroclastic textured rocks originated at intermediate depths (Kil and Wendlandt 2004).

The methods utilized to define the boundary between lithosphere and asthenosphere, including seismic data, chemical data, and isotopic data, indicate that the boundary is currently located near the base of the crust along the Rio Grande rift axis (Perry et al. 1987; Baldridge et al. 1995). This boundary closely corresponds to that for the depths of origin of undeformed (protogranular) and deformed (porphyroclastic and equigranular) rocks. Protogranular texture rocks were not found on the rift shoulder (Adam's Diggings), but these rocks could have existed at depths greater than

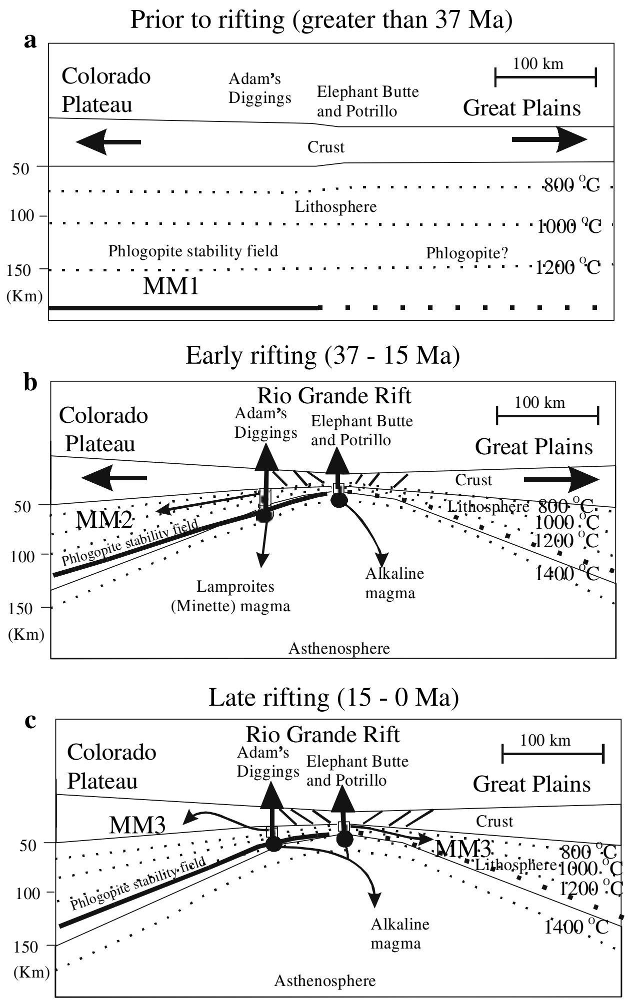

Fig. 10 **a–c** A schematic history of lithosphere evolution in the Rio Grande rift. MM1, MM2 and MM3 are first, second, and third mantle metasomatic events, respectively. **a** Prior to rifting (greater than 37 Ma), temperature distributions based on 44 mWm^{-2} geotherm (Pollack and Chapman 1977), **b** Early rifting (37–15 Ma), and **c** late rifting (15–0 Ma). The boundary of the phlogopite stability field is based on Sato et al. (1996)

about 60 km at the time of eruption (Kil and Wendlandt 2004).

The phlogopite stability field changed as the lithosphere thinned, commensurate with changing pressure and temperature conditions (Fig. 10b). Prior to rifting, phlogopite was stable at depths shallower than about 190 km (44 mW/m^2, Sato et al. 1996). After rifting commenced, however, the phlogopite stability field evolved with changing geothermal gradients. By 15 Ma, phlogopite was stable in the mantle under Adam's Diggings only at depths shallower than about 61 km (18.5 kb) at 1,125 °C (Wendlandt and Eggler 1980).

Partial melting under the rift shoulder may have been triggered by the dehydration melting of hydrous minerals, amphibole and perhaps phlogopite, to form alkaline series rocks, including minettes (Wendlandt and Eggler 1980), whereas decompression melting is the primary mechanism for melt generation in the rift axis (Fig. 10b). The second episode of mantle metasomatism (MM2), giving rise to LREE and other incompatible element enrichments in clinopyroxene and, possibly, crystallization of phlogopite on the rift shoulder, involved a minette-type melt with high LREE contents (Fig. 10b). There is no evidence of MM2 metasomatism along the rift axis during this period.

Late rifting (middle Miocene to Holocene; 15–0 Ma)

After early Miocene, the mantle under the southern Rio Grande rift broadly started cooling (Bussod and Williams 1991) with resulting development of reequilibration textures in minerals. Evidence of earlier high temperature conditions followed by cooling include exsolution lamellae of orthopyroxene in clinopyroxene, and vice versa, and slightly changing Al contents of porphyroclastic orthopyroxene cores relative to neoblastic rims (Kil and Wendlandt 2004). The temperature difference between initial equilibration and subsequent cooling was larger in deformed rocks (porphyroclastic and equigranular textures) than in undeformed rocks (protogranular texture) in the rift axis.

During the later phase of magmatism (middle Miocene–Holocene) in the Rio Grande rift, volcanic activity was generally associated with the northeast trending Jemez Lineament, extending from the San Carlos volcanic field in eastern Arizona to the Raton-Clayton volcanic field of northeastern New Mexico (Perry et al. 1987; Fig. 1). The melts that erupted away from this lineament in the southern Rio Grande rift, therefore, likely formed as independent, isolated batches by local thermal perturbations. During this period, localized alkaline magmas at Adam's Diggings, Elephant Butte, and Potrillo brought mantle xenoliths to the surface at 12.6, 2.9 Ma, and 80 Ka, respectively. Mantle metasomatism (MM3) involving the host melts or melts of similar composition (alkali basalt and basanite magmas) modified xenolith compositions from the rift axis and possibly those from the rift shoulder (Fig. 10c). The phlogopite stability field during late rifting was similar to that during the early rifting period (Fig. 10c). Partial melting at Adam's Diggings may have been triggered by phlogopite dehydration (Fig. 10c).

Acknowledgments We thank Ian Ridley (US Geological Survey in Denver) for providing access to the LA-ICPMS facility and Charlie Blount for assistance with the Colorado School of

Mines microprobe. Critical reviews by Michael Roden, Doug Smith, Craig Simmons, and Greg Holden are appreciated.

References

Adam J, Green TH (1994) The effects of pressure and temperature on the partitioning of Ti, Sr, and REE between amphibole, clinopyroxene and basanitic melts. Chem Geol 117:219–233

Aldrich MJJr, Chapin CE, Laughlin AW (1986) Stress history and tectonic development of the Rio Grande rift, New Mexico. J Geophys Res 91:6199–6211

Bachman GO, Mehnert HH (1978) New K-Ar dates and the late Pliocene to Holocene geomorphic history of the central Rio Grande region, New Mexico. Geol Soc Am Bull 89:283–292

Baldridge WS (1979) Mafic and ultramafic inclusion suites from the Rio Grande rift (New Mexico) and their bearing on the composition and thermal state of the lithosphere. J Volcanol Geotherm Res 6:319–351

Baldridge WS, Damon PE, Shafiqullah M, Bridwell RJ (1980) Evolution of the central Rio Grande rift, New Mexico: new potassium–argon ages. Earth Plant Sci Lett 51:309–321

Baldridge WS, Olsen KH, Callender JF (1984) Rio Grande rift: problems and perspectives. N M Geol Soc Guidebook 35:1–12

Baldridge WS, Perry FV, Vaniman DT, Nealey LD, Leavy BD, Laughlin AW, Kyle P, Bartow Y, Steinitz G, Gladney ES (1991) Middle to late Cenozoic magmatism of the southeastern Colorado Plateau and central Rio Grande rift (New Mexico and Arizona, USA): a model for continental rifting. Tectonophysics 197:327–354

Baldridge WS, Keller GR, Haak V, Wendlandt E, Jiracek GR, Olsen KH (1995) The Rio Grande rift, In: Olsen KH (ed) Continental rifts: evolution, structure, tectonic. Elsevier, Amsterdam, pp 233–275

Beccaluva L, Bonadiman C, Coltorti M, Salvini L, Siena F (2001) Depletion event, nature of metasomatizing agent and timing of enrichment processes in lithospheric mantle xenoliths from the Veneto volcanic province. J Petrol 42:173–187

Bonatti E, Ottonello G, Hamlyn PR (1986) Peridotites from Island of Zabargad (St John) Red Sea: petrology and geochemistry. J Geophys Res 91:599–631

Brown GC, Mussett AE (1981) The inaccessible Earth. Allen & Unwin, London, pp 235

Bussod GYA, Williams DR (1991) Thermal and kinematic model of the southern Rio Grande rift: inferences from crustal and mantle xenoliths from Kilbourne Hole, New Mexico. Tectonophysics 197:373–389

Carlson, RW, Nowell, GM (2001) Olivine-poor sources for mantle-derived magmas: Os and Hf isotopic evidence from potassic magmas of the Colorado Plateau. Geochem Geophys Geosys 2. Paper number 2000GC000128

Coltorti M, Bonadiman C, Hinton RW, Siena F, Upton BGJ (1999) Carbonatite metasomatism of the oceanic upper mantle: evidence from clinopyroxenes and glasses in ultramafic xenoliths of Grande Comore, Indian Ocean. J Petrol 40:133–165

Dawson JB (1984) Contrasting types of upper mantle metasomatism? In: Kornprobst J (ed) Kimberlites II. Elsevier, Amsterdam, pp 289–294

Fedorowich JS, Richards JP, Jain JC, Kerrich R, Fan J (1993) A rapid method for REE and trace-element analysis using laser sampling ICP-MS on direct fusion whole-rock glasses. Chem Geol 106:229–249

Frey FA, Green DH (1974) The mineralogy, geochemistry and origin of lherzolite inclusions in Victorian basanites. Geochim Cosmochim Acta 49:2469–2491

Frey FA, Prinz M (1978) Ultramafic inclusions from San Carlos, Arizona: petrologic and geochemical data bearing on their petrogenesis. Earth Planet Sci Lett 38:129–176

Gamble JA, McGibbon F, Kyle PR, Menzies MA, Kirsch I (1988) Metasomatised xenoliths from Foster Crater, Antarctica: implications for lithospheric structure and processes beneath the Transantarctic Mountain Front. J Petrol Spec Lithosphere Issue, pp 109–138

Griffin WL, O'Reilly SY, Ryan CG, Gaul O, Ionov D (1998) Secular variation in the composition of subcontinental lithospheric mantle. In: Braun J et al (ed) Structure and evolution of the Australian continent. American Geophysical Union, Geodynamics Series 26:1–25

Halliday A, Lee D-C, Tommasini S, Davies GR, Paslick CR, Fitton JG, James DE (1995) Incompatible trace elements in OIB and MORB and source enrichment in the sub-oceanic mantle. Earth Planet Sci Lett 133:379–395

Hamilton DL, Bedson P, Esson J (1989) The behavior of trace element in the evolution of carbonatites. In: Bell K (ed) Carbonatites-Genesis and evolution, Unwin Hyman, London, pp 405–427

Hofmann AW (1988) Chemical differentiation of the Earth: the relationship between mantle, continental crust, and oceanic crust. Earth Planet Sci Lett 90:297–314

Johnson KE, Davis AM, Bryndzia LT (1996) Contrasting styles of hydrous metasomatism in the upper mantle: an ion microprobe investigation. Geochim Cosmochim Acta 60:1367–1385

Kelemen P, Shimizu N, Dunn T (1993) Relative depletion of niobium in some magmas and the continental crust: partitioning of K, Nb, La and Ce during melt/rock reaction in the upper mantle. Earth Planet Sci Lett 120:111–134

Kil Y (2002) Mantle evolution associated with the Rio Grande rift: Geochemistry and geothermobarometry of upper mantle xenoliths. PhD dissertation, Colorado School of Mines, Golden, pp 160

Kil Y, Wendlandt RF (2004) Pressure and temperature evolution of upper mantle under the Rio Grande rift. Contrib Mineral Petrol 148:265–280

Kyser TK, Rison W (1982) Systematics of rare gas isotopes in basic lavas and ultramafic xenoliths. J Geophys Res 87:5611–5630

Leeman WP (1982), Tectonic and magmatic significance of strontium isotopic variations in Cenozoic volcanic rocks from the western Unites States. Geol Soc Am Bull 93:487–503

Lichte FE (1995) Determination of elemental content of rocks by laser ablation inductively coupled plasma mass spectrometry. Anal Chem 67:2479–2485

Maalöe S, Aoki K (1977) The major element composition of upper mantle estimated from the composition of lherzolites. Contrib Mineral Petrol 63:161–173

Mattery DP, Menzies M, Pillinger CT (1985) Carbon isotopes in lithosphere peridotites and pyroxenites. Terra Cognita 5:147

McKenzie D (1985) The extraction of magma from the crust and mantle. Earth Planet Sci Lett 74:81–91

McKenzie D, O'Nions RK (1991) Partial melt distributions from inversion of rare earth element concentrations. J Petrol 32:1021–1091

McMillan NJ, Dickin AP, Haag D (2000) Evolution of magma source regions in the Rio Grande rift, southern New Mexico. Geol Soc Am Bull 112:1582–1593

Menzies M, Kempton P, Dungan M (1985) Interaction of continental lithosphere and asthenospheric melts below the Geronimo volcanic field, Arizona, USA. J Petrol 26:663–693

Menzies MA, Hawkesworth CJ (1987) Mantle metasomatism. Academic, London, pp 472

Menzies MA, Arculus RJ, Best MG, Bergman SC, Ehrenberg SN, Irving AJ, Roden MF, Schulze DJ (1987) A record of subduction processes and within-plate volcanism in lithospheric xenoliths of the southwestern USA. In: Nixon PH (ed) Mantle xenoliths, Wiley, New York, pp 59–74

Nagasawa H, Schreiber HD, Morris RV (1980) Experimental mineral/liquid partition coefficients of rare earth elements (REE), Sc and Sr for perovskite, spinel and melilite. Earth Planet Sci Lett 46:431–437

Nicholls IA (1974) A direct fusion method of preparing silicate rock glasses for energy dispersive electron microprobe analysis. Chem Geol 14:151–157

Nicholls IA, Harris KL (1980) Experimental rare earth element partition coefficients for garnet, clinopyroxene and amphibole coexisting with andesitic and basaltic liquids. Geochim Cosmochim Acta 44:287–308

Nixon PH (1987) Mantle xenoliths. Wiley, New York, pp 844

Norman MD (1998) Melting and metasomatism in the continental lithosphere: laser ablation ICPMS analysis of minerals in spinel lherzolites from eastern Australia. Contrib Mineral Petrol 130:240–255

O'Reilly SY, Griffin WL (1988) Mantle metasomatism beneath western Victoria, Autralia: I. Metasomatic processes in Cr-diopside lherzolites. Geochim Cosmochim Acta 52:433–448

Perry FV, Baldridge WS, DePaolo DJ (1987) Role of asthenosphere and lithosphere in the genesis of late Cenozoic basaltic rocks from the Rio Grande rift and adjacent regions of the southwestern United States. J Geophys Res 92:9131–9213

Pollack HN, Chapman DS (1977) On the regional variation of heat flow, geotherms and lithospheric thickness. Tectonophysics 38:279–296

Ridley WI, Lichte FE (1998) Major, trace, and ultratrace element analysis by laser ablation ICP-MS. Rev Econ Geol 7:199–215

Roden MF, Murthy VR (1985) Mantle metasomatism. Ann Rev Earth Planet Sci 13:269–296

Roden MF, Shimizu N (1993) Ion microprobe analyses bearing on the composition of the upper mantle beneath the Basin and Range and Colorado Plateau provinces. J Geophys Res 98:14091–14108

Roden MF, Irving AJ, Murthy VR (1988) Isotopic and trace element composition of the upper mantle beneath a young continental rift: results from Kilbourne Hole, New Mexico. Geochim Cosmochim Acta 52:461–473

Sato K, Katsura T, Ito E (1996) Phase relation of phlogopite with and without enstatite up to 8 Gpa: implication to potassic magmatism and mantle metasomatism. Tech Rep of ISEI, Ser A 65:8

Sengor AHC, Burke K (1978) Relative timing of rifting and volcanism in earth and its tectonic implications. Geophs Res Lett 5:419–421

Solomon M (1963) Counting and sampling errors in modal analysis by point counter. J Petrol 4:367–382

Stosch HG (1982) Rare earth element partitioning between minerals from anhydrous spinel peridotite xenoliths. Geochim Cosmochim Acta 46:793–811

Stix J, Gauthier G, Ludden JN (1995) A critical look at quantitative laser-ablation ICP-MS analysis of natural and synthetic glasses. Can Mineral 33:435–444

Sun SS, McDonough WF (1989) Chemical and isotopic systematics of oceanic basalt: implications for mantle composition and processes. In: Saunders AD, Norry MJ (eds) Magmatism in ocean basins. Geol Soc London Spec Pub 42:313–345

Vaniman D, Laughlin AW, Gladney ES (1985) Navajo minettes in the Cerros de las Mujeres, New Mexico. Earth Planet Sci Lett 74:69–80

Warren RG (1978) Characterization of the lower crust-upper mantle of the Engle basin, Rio Grande rift, from a petrochemical and field geologic study of basalts and their inclusions. MS thesis. University of New Mexico, Albuquerque, pp156

Warren RG, Kudo AM, Keil K (1979) Geochemistry of lithic and single-crystal inclusions in basalt and a characterization of the upper mantle-lower crust in the Engle basin, Rio Grande rift, New Mexico. In: Riecker RE (ed) Rio Grande rift: tectonics and magmatism. American Geophysical Union Special Publication, Washington, pp 393–415

Wendlandt RF, Harrision WJ (1979) Rare earth partitioning between immiscible carbonate and silicate liquids and CO_2 vapor: results and implications for the formation of light rare earth-enriched rocks. Contrib Mineral Petrol 69:409–419

Wendlandt RF, Eggler DH (1980) The origins of potassic magmas: 2. stability of phlogopite in natural spinel lherzolite and in the system $KAlSiO_4$–MgO–SiO_2–H_2O at high pressures and high temperatures. Am J Sci 280:421–458

Wendlandt RF, Altherr R, Neumann E-R, Baldridge WS (1995) Petrology, geochemistry, isotopes. In: Olsen KH (ed) Continental rifts: evolution, structure, tectonics. Elsevier, Amsterdam, pp 47–60

Witt-Eickschen G, Seck HA (1987) Temperature of sheared mantle xenoliths from the West Eifel, West Germany: evidence for mantle diapirism beneath the Rhenish massif. J Petrol 28:475–493

Wyllie PJ (1977) Mantle fluid composition buffered in peridotite–CO_2–H_2O by carbonates, amphibole and phlogopite. J Geol 86:687–713

Xu X, O'Reilly SY, Griffin WL, Zhou X (2000) Genesis of young lithospheric mantle in southern China: an LAM-ICPMS trace element study. J Petrol 41:111–148

Yaxley GM, Crawford AJ, Green DH (1991) Evidence for carbonatite metasomatism in spinel peridotites from western Victoria Australia. Earth Planet Sci Lett 197:305–317

Zipfel J, Wörner G (1992) Four-and five-phase peridotites from a continental rift system: evidence for upper mantle uplift and cooling at the Ross Sea margin (Antarctica). Contrib Mineral Petrol 111:24–36